JACS
JOURNAL OF THE AMERICAN CHEMICAL SOCIETY
Article
Cite This: J. Am. Chem. Soc. 2018, 140, 6978−6983
pubs.acs.org/JACS

Accurate Measurement of Residual Dipolar Couplings in Large RNAs by Variable Flip Angle NMR

Jan Marchant,*,† Ad Bax,§ and Michael F. Summers*,†,‡

†Department of Chemistry and Biochemistry and ‡Howard Hughes Medical Institute, University of Maryland Baltimore County (UMBC), Baltimore, Maryland 21250, United States

§Laboratory of Chemical Physics, National Institute of Diabetes, Digestive and Kidney Diseases, National Institutes of Health, Bethesda, Maryland 20892, United States

Supporting Information

ABSTRACT: NMR approaches using nucleotide-specific deuterium labeling schemes have enabled structural studies of biologically relevant RNAs of increasing size and complexity. Although local structure is well-determined using these methods, definition of global structural features, including relative orientations of independent helices, remains a challenge. Residual dipolar couplings, a potential source of orientation information, have not been obtainable for large RNAs due to poor sensitivity resulting from rapid heteronuclear signal decay. Here we report a novel multiple quantum NMR method for RDC determination that employs flip angle variation rather than a coupling evolution period. The accuracy of the method and its utility for establishing interhelical orientations are demonstrated for a 36-nucleotide RNA, for which comparative data could be obtained. Applied to a 78 kDa Rev response element from the HIV-1 virus, which has an effective rotational correlation time of ca. 160 ns, the method yields sensitivity gains of an order of magnitude or greater over existing approaches. Solution-state access to structural organization in RNAs of at least 230 nucleotides is now possible.

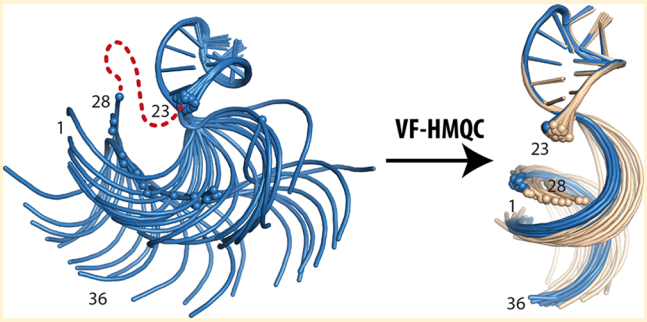

INTRODUCTION

RNAs participate in a diverse and growing number of known biological functions.[1] Like proteins, RNA function is dependent on structure, both of which can be modulated by effectors such as metabolites, proteins, and ions. However, compared to proteins, knowledge about RNA structure and the determinants of folding remain limited. Approximately 4500 RNA structures have been deposited in the Nucleic Acid Database (NDB), compared to more than 135,000 protein depositions in the Protein Databank (PDB). In part, this relative paucity can be explained by difficulties in applying common biophysical techniques to RNA. Conformational heterogeneity and flexibility can cause crystallization challenges and complicate analysis by electron microscopy. NMR approaches for medium-to-large RNAs are challenging due to low chemical shift dispersion, low proton density, lack of NOEs between secondary structure elements, and large $^{13}C-^{1}H$ dipolar coupling that severely limits the sensitivity of heteronuclear correlation experiments.[2−4]

Recent advances in deuterium labeling have provided routes to overcome several of the NMR challenges.[5−8] Nucleotide-specific ^{2}H-editing can alleviate spectral crowding and decrease line widths, allowing chemical shift assignment and determination of interproton distances using nuclear Overhauser effect (NOE) spectroscopy. Although NOEs provide high resolution local structural information, they cannot define relative orientations of distinct secondary structure elements, such as distinct helices, except in the rare cases where long-range NOEs can be observed (e.g., at sites of long-range A-minor contacts[9]). An approach that works well for proteins and has been applied to relatively small RNAs involves NMR detection of residual dipolar couplings (RDCs).[5,9−18] In solution, dipole−dipole interactions between nuclei average to zero due to rapid molecular reorientation. However, upon introduction of a medium that causes a small degree of solute alignment, the dipole−dipole interaction is no longer fully averaged. The sign and magnitude of the resulting RDC are dependent on the time-averaged angle between the internuclear vector and the external field. Given sufficient RDCs, the alignment tensor and the relative orientation of each internuclear vector can be calculated,[19−21] thereby providing long-range orientation restraints. Larger RNAs present unique challenges for RDC measurement due to severe ^{1}H NMR line broadening that occurs upon incorporation of ^{13}C nuclei. As such, a recently developed method for measuring RDCs in RNAs from TROSY intensities becomes impractical for RNAs with rotational correlation times longer than 30 ns.[22]

We have developed an approach that exploits the relatively large chemical shift dispersion and slow relaxation rates of the

Received: March 26, 2018
Published: May 14, 2018

DOI: 10.1021/jacs.8b03298
J. Am. Chem. Soc. 2018, 140, 6978−6983

adenosine H2 protons. Even in large RNAs, the H2 signals remain sharp,[5−8] provided that the RNA is dissolved in D_2O such that the uridine N3 position is deuterated. Under these conditions, the H2 is relatively well isolated from sources of relaxation, with the closest proton ∼5 Å away for Watson−Crick base pairs in regular A-helical geometry. Since isotopic enrichment with ^{13}C leads to severe line broadening due to a strong dipolar interaction, our experiments are applied to RNAs that contain uniformly ^{15}N-enriched adenosines. Adenosine N1 and N3 nuclei have a negligible effect on relaxation of the H2 proton due to their relatively low gyromagnetic ratio and internuclear separation of ∼2 Å. The two-bond H2−N1 and H2−N3 scalar couplings (∼14.5 Hz[23]) are sufficient to allow recording of high quality $^{15}N-^{1}H$ SOFAST-HMQC spectra,[24,25] which suggested to us that we may be able to utilize the H2−N1 and H2−N3 couplings in adenosines to measure RDCs in large RNAs.

RESULTS AND DISCUSSION

The residual dipolar coupling, D_{IS}, between two spins, I and S, is given in Hz by[26]

$$D_{IS} = -\frac{\mu_0 \gamma_I \gamma_S \hbar}{4\pi^2 r_{IS}^3} \left\langle \frac{3\cos^2\theta - 1}{2} \right\rangle \quad (1)$$

where the angular brackets denote time or ensemble averaging, μ_0 is the vacuum permeability, $\hbar$ is the reduced Planck constant, γ_I is the magnetogyric ratio of nucleus I, r_{IS} is the internuclear distance, and θ is the angle between the internuclear vector and the external magnetic field. The relatively large internuclear distance (2.06 Å[32]) means that the dipolar interaction will be small compared to more commonly measured one-bond couplings. Using a commonly targeted 0.1% alignment, the expected range for adenosine $^{2}D_{NH}$ RDCs is ∼5 Hz, although, due to the relatively isolated H2, higher degrees of alignment may be possible without the usual complications due to $^{1}H-^{1}H$ RDCs.[33] This will be limited by H2−H2 RDCs in stacked adenosines, which will have similar magnitudes to the H2−N1 and H2−N3 couplings. The relative angle of H2−N1 and H2−N3 internuclear vectors is fixed by adenine's geometry at ∼72°,[32] making them highly complementary.

We initially focused on a 232-nucleotide HIV-1 Rev response element RNA construct engineered to adopt one of two equilibrium conformations (RRE^{232A}).[34] Well-dispersed signals indicative of regular secondary structure were readily detected using the SOFAST-HMQC. However, attempts to apply an existing spin-state selective (S^3E)[31] experiment for measuring H2−N1/N3 couplings were unsuccessful (Figure 1C) due to rapid relaxation of transverse ^{15}N magnetization during the time period necessary for separating antiphase components. The relatively small $^{2}J_{NH}$ coupling (∼14.5 Hz) requires ^{15}N magnetization to be transverse for approximately 17 ms during the S^3E element.[35] Experimentally, we find N3 $T_{1\rho}$ values below 5 ms for RRE^{232A} at 600 MHz and 308 K (Supporting Information Figure S1), corresponding to an effective rotational correlation time of ca. 160 ns, under the assumption that chemical shift anisotropy (CSA) is the dominant relaxation mechanism and using a CSA value of 330 ppm.[36] We would expect to lose more than 95% of this signal during the S^3E element, essentially rendering it undetectable for practical purposes.

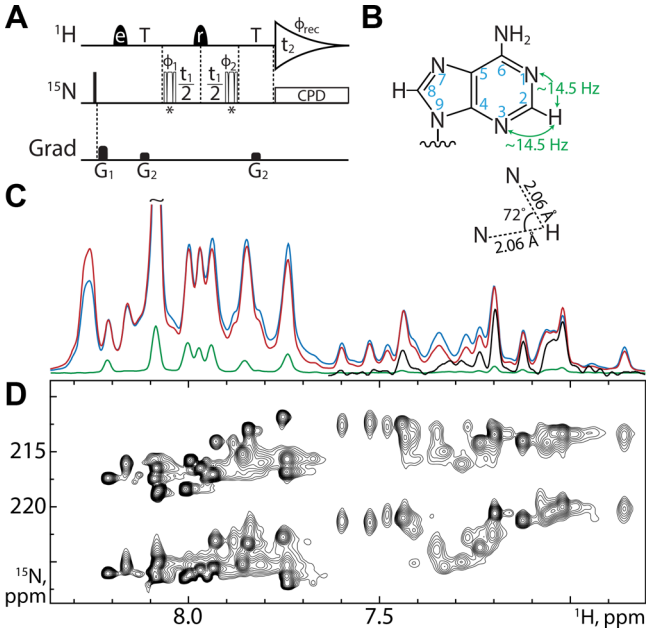

Figure 1. (A) VF-HMQC pulse sequence for measurement of $^{2}D_{NH}$ in adenine bases. Narrow bars represent 90° pulses, while half-ellipsoids denote shaped ^{1}H pulses, with e and r representing EBURP2 and ReBURP pulses, respectively.[27] ^{15}N pulses marked * are BIR-4 pulses[28] designed for either 90 or 45° flip angles, applied in an interleaved manner. ^{1}H shaped pulses have a duration of 2.8 ms (EBURP) and 3 ms (ReBURP) at 600 MHz and are centered at 7.4 ppm. ^{15}N pulses are applied at 220 ppm. All pulses have phase x unless otherwise indicated. The delay T is set to $1/(3J_{NH})$ (22.73 ms). Phase cycling: $\phi_1 = x, -x$, $\phi_2 = x, x, -x, -x$, $\phi_{rec} = x, -x, -x, x$. Gradient pulses $G_{1,2}$ = 5.8, 3.75 G/cm with durations of 1 ms. All gradient pulses are smoothened rectangular shapes. Quadrature detection is achieved using the STATES-TPPI method with ϕ_1 incremented by 90° for each FID.[29] Composite pulse decoupling is achieved using the GARP sequence.[30] (B) Adenine geometry. Magnetization is transferred via the two-bond coupling between H2 and N1/N3 as indicated. The relative angle between the H2−N1 and H2−N3 internuclear vectors is 72°. (C) VF-HMQC with 90° flip (red), SOFAST-HMQC[24,25] (blue), and S^3E[31] (green) experiments recorded on the 232-nucleotide RRE^{232A} without ^{15}N chemical shift evolution shows the increase in sensitivity of our approach. The upfield region of the S^3E experiment is scaled up by 10 times in black. (D) VF-HMQC spectrum of RRE^{232A} showing H2−N1 and H2−N3 correlations.

To address this issue, we first considered a quantitative J style experiment.[37] However, this is complicated by concurrent evolution of both H2−N1 and H2−N3 couplings during the dephasing/rephasing delays. Selective ^{15}N pulses to determine the individual contribution of N1 and N3 are rendered impractical by their poor frequency separation (Figure 1D) and rapid ^{15}N relaxation during the requisite long shaped pulses. It is possible to reduce the contribution of the passive coupling using a small heteronuclear flip angle.[38−40] However, significant reduction requires flip angles as low as 20° (Supporting Information Figure S2A), leading to signal loss of nearly 90%.

The intensity $s(t_1, t_2)$ of an HMQC signal obtained for a flip angle ϕ of the heteronuclear pulses, and de/rephasing delays of duration τ, for the case where the detected spin I is coupled to two heteronuclear spins S and T and assuming $J_{ST} = 0$ is given by

DOI: 10.1021/jacs.8b03298
J. Am. Chem. Soc. 2018, 140, 6978−6983

$$s(t_1, t_2) = e^{i\Omega_I t_2} s^2(\phi) \{e^{i\Omega_S t_1} s^2(\pi J_{IS}\tau)[c^2(\pi J_{IT}\tau) + s^2(\pi J_{IT}\tau)c^2(\phi)] + e^{i\Omega_T t_1} s^2(\pi J_{IT}\tau)[c^2(\pi J_{IS}\tau) + s^2(\pi J_{IS}\tau)c^2(\phi)]\} \quad (2)$$

with c and s representing cosine and sine functions, respectively. Following Fourier transform, this yields a signal at (Ω_S, Ω_I) with intensity $\mathcal{I}_\phi$ given by

$$\mathcal{I}_\phi = \sin^2(\phi) \sin^2(\pi J_{IS}\tau)[\cos^2(\pi J_{IT}\tau) + \sin^2(\pi J_{IT}\tau) \cos^2(\phi)] \quad (3)$$

It is apparent that the variable flip angle modulates both the total intensity and the contribution of the passive spin coupling to the final signal. The contribution of the actively coupled spin can therefore be removed by taking the ratio of two experiments where the flip angle is varied (Supporting Information Figure S2). For nearly optimal flip angles of 45 and 90° (Supporting Information Figure S3), this ratio (R_S) is given by

$$R_S = \frac{\mathcal{I}_{45}}{\mathcal{I}_{90}} = \frac{\tan^2(J_{IT}\pi\tau) + 2}{4} \quad (4)$$

The couplings can then be found from the intensity ratio using

$$J_{IT} = \frac{\text{atan}(\sqrt{4R_S - 2})}{\pi\tau} \quad (5)$$

The analysis presented thus far assumes that the ^{15}N pulses are perfectly calibrated and homogeneous across the sample. In general, the B_1 field is not homogeneous. We therefore used a pair of BIR-4 adiabatic pulses, designed to be insensitive to B_1 miscalibration and inhomogeneity,[28,41] which are exceptionally robust (Supporting Information Figure S4). The final pulse sequence used for measurement of the couplings in this work therefore consists of an HMQC in which the ^{15}N pulses are replaced by BIR-4 pulses, with flip angles of 45 and 90° applied in an interleaved fashion. Any ^{1}H−^{1}H RDCs with imino or ribose protons are refocused by the application of a band-selective ReBURP pulse[27] at the midpoint of the t_1 evolution period. Even though the small amount of ^{1}H−^{1}H dephasing due to H2−H2 RDCs in stacked adenosines cannot be refocused using band-selective pulses, its effect is the same for both spectra and therefore does not impact the size of the extracted coupling. We call this experiment a variable flip HMQC (VF-HMQC) (Figure 1A). The pulse sequence for Bruker spectrometers is included as Supporting Information.

We applied the VF-HMQC sequence to RRE^{232A} and compared the sensitivity to SOFAST-HMQC and S^{3}E experiments, in each case removing the ^{15}N chemical shift evolution period (Figure 1C). As expected on the basis of its similar pulse sequence structure, the sensitivity of our new approach is comparable to the SOFAST-HMQC, whereas the S^{3}E experiment is less sensitive by at least 10-fold, with many signals completely undetectable. A 21 h VF-HMQC acquisition using 160 μL of ∼1.5 mM RRE^{232A} with ^{15}N chemical shift evolution (Figure 1D) gives a S/N ratio for the weakest, fast relaxing signals of ∼50:1 in the 90° flip angle experiment.

The uncertainty in R_S is given by

$$\sigma_R = \frac{N\sqrt{R_S^2 + 1}}{\mathcal{I}_{90}} \quad (6)$$

where N is the root-mean-square noise in the spectrum. The uncertainty in J then follows from

$$\frac{\partial J_{IT}}{\partial R_S} = \frac{2}{\pi\tau\sqrt{4R_S - 2}\,(4R_S - 1)} \quad (7)$$

to yield

$$\sigma_J = \frac{2N\sqrt{R_S^2 + 1}}{\mathcal{I}_{90}\pi\tau\sqrt{4R_S - 2}\,(4R_S - 1)} \quad (8)$$

as detailed in Supporting Information Appendix 1. The optimum value for τ to minimize σ_J is a function of the total coupling. The most important consideration is to avoid approaching $\tau = 1/(2J)$ where $\mathcal{I}_{90} = 0$. Graphical analysis

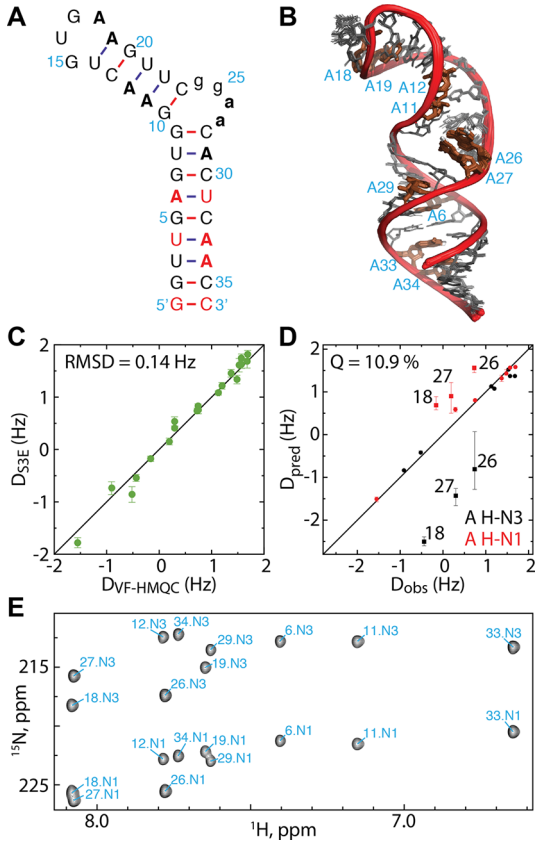

Figure 2. (A) SLC^A RNA construct used to validate the VF-HMQC method. Adenosines are shown in bold. Non-native residues are shaded in red. Residues from the interhelical bulge omitted in some calculations are shown in lower case. (B) Ensemble of 20 lowest energy structures of SLC^A, calculated using NOE and ^{13}C−^{1}H RDC restraints. (C) Comparison of $^2D_{NH}$ for SLC^A adenosines measured using the VF-HMQC and S^{3}E approaches, showing good correlation (RMSD = 0.14 Hz). Error bars for each experiment indicate uncertainty due to noise and line width. (D) Observed $^2D_{NH}$ values for SLC^A obtained using VF-HMQC are well correlated with back-calculated RDCs from the ensemble shown in part B (Q = 10.9%). Loop and bulge adenosines are labeled and omitted from the Q value calculation. Error bars for D_{pred} represent the maximum and minimum RDCs calculated for the ensemble. (E) Assigned VF-HMQC spectrum for SLC^A.

DOI: 10.1021/jacs.8b03298
J. Am. Chem. Soc. 2018, 140, 6978−6983

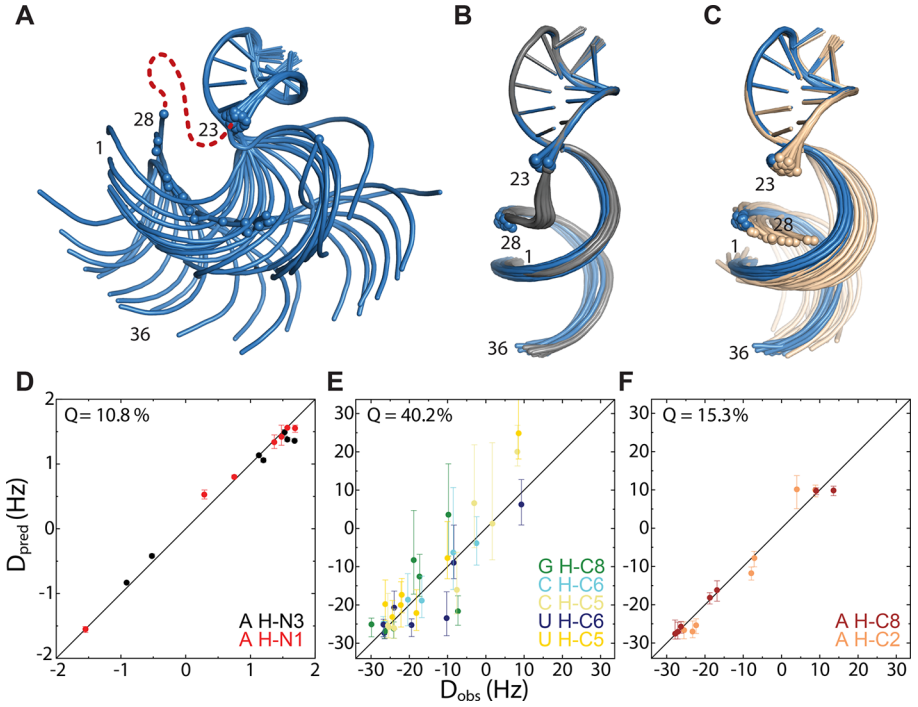

Figure 3. (A) Ensemble of the 20 lowest energy SLC^{A} structures calculated using NOEs but without residues from the interhelical bulge. The relative orientation of the helices is not well-defined, with interhelical angles ranging from −83 to 110°. (B) In blue, like part A but with incorporation of 47 ^{13}C−^{1}H RDC restraints. The interhelical angle is between 76 and 84° (M = 81.5°, SD = 2.6°). This agrees well with the ensemble calculated for the full RNA, shown in gray. (C) In cream, like A but with addition of 14 ^{15}N−^{1}H RDCs measured with the VF-HMQC approach. These RDCs are sufficient to restrain the interhelical angle between 77 and 94° (M = 84°, SD = 4.1°), in agreement with part B, overlaid in blue. (D) Observed ^{15}N−^{1}H RDCs plotted against those back-calculated for the ensemble calculated with ^{13}C−^{1}H RDCs, shown in blue in part B. Error bars for D_{pred} represent the maximum and minimum RDCs calculated for the ensemble. (E) Observed ^{13}C−^{1}H RDCs for guanosine, cytidine, and uridine residues plotted against those back-calculated for the ensemble calculated with ^{15}N−^{1}H RDCs, shown in cream in part C. (F) Observed ^{13}C−^{1}H RDCs for adenosine residues plotted against those back-calculated for the ensemble calculated with ^{15}N−^{1}H RDCs, shown in cream in part C.

indicates that choosing $\tau = 1/(3J)$ yields uncertainties of <0.2 Hz for the range of expected $^{2}(J + D)_{NH}$ values for a S/N ratio of 50:1, as measured for RRE^{232A} (Supporting Information Figure S5). The RDC is calculated from the difference in couplings measured under isotropic and aligned conditions and will therefore have an uncertainty of $\sim\sqrt{2}\sigma_J$ assuming the same S/N in both experiments, suggesting a total uncertainty of <0.3 Hz is attainable. This uncertainty is more than an order of magnitude smaller than the expected range of the RDCs and as such is anticipated to have a negligible effect during fitting compared to the uncertainty in the coordinates of the reference structure.[42]

From ∼80 resolved signals in the RRE^{232A} HMQC, we were able to measure 62 $^{2}J_{NH}$ values with uncertainties <0.2 Hz (M = 14.7 Hz, SD = 0.24 Hz; uncertainties for the remaining signals were higher due to lower S/N). Following alignment with ∼13 mg/mL Pf1 phage, we measured 59 RDCs with uncertainties <0.3 Hz, ranging from −0.9 to 2.7 Hz. As there is no comparable method for measuring these couplings in large RNAs, it is not possible to directly validate these measurements. Instead, we designed a 36-nt RNA construct based on stem loop C from the MMLV 5′-Leader (SLC^{A}, Figure 2A). This RNA contains two helices separated by a noncanonical *k*-turn[5] which leads to an interhelical angle of ∼74°.[43] We engineered three additional A:U base pairs into the proximal helix so that each helix contained at least six H2−N RDCs (Figure 2A). Excellent agreement was observed between 20 ^{15}N−^{1}H RDCs calculated using the VF-HMQC (Figure 2E) and S^{3}E (Supporting Information Figure S6) approaches (Pearson correlation coefficient = 0.992; RMSD = 0.14 Hz; Figure 2C), which confirmed the accuracy of the VF-HMQC approach.

We next wished to determine if the H2−N1/3 RDCs were sufficient to independently establish the interhelical angle in SLC^{A}. A total of 47 H2−C2, H8−C8, H5−C5, and H6−C6 RDCs were measured using the ARTSY approach[22,44] (Supporting Information Figure S7), which were used together with 262 distance restraints to calculate a structural ensemble for this construct (Figure 2B). Back-calculated RDCs from this structure ensemble correlate exceptionally well with ^{15}N−^{1}H RDCs measured using the VF-HMQC approach for the helical regions (Q = 10.9%, Figure 2D), despite not having been used as input parameters.

The presence of multiple long-range NOEs from residues in the interhelical bulge to helix 2 leads to a relatively well-defined interhelical angle, even in the absence of RDC restraints. To better assess the ability of the RDCs to determine interhelical angles, we calculated an ensemble of SLC^{A} structures in which the bulge residues were substituted by a long chain of pseudoatoms, thus removing interhelical distance and geometric constraints. In the absence of RDCs, the relative orientation of the two helices is poorly defined (Figure 3A, Supporting Information Figure S8). Upon refinement with ^{13}C−^{1}H RDC restraints (Figure 3B), the interhelical angle is well-defined (between 76 and 84°) and shows a good correlation with the measured ^{15}N−^{1}H RDCs (Q = 10.8%,

DOI: 10.1021/jacs.8b03298
J. Am. Chem. Soc. 2018, 140, 6978−6983

Figure 3D). Importantly, refinement with the 14 $^{15}N-^{1}H$ RDCs measured using the VF-HMQC approach (and without the $^{13}C-^{1}H$ RDCs) also affords structures with a well-defined interhelical angle (between 77 and 94°) that is in good agreement with both of the models derived using $^{13}C-^{1}H$ RDCs and the original SLC^{A} structure (Figure 3C). Agreement with the measured $^{13}C-^{1}H$ RDCs remains good (overall Q = 34.8%), although the correlation is weaker for non-adenosine residues (Q = 40.2%, Figure 3D) than for the adenosines (Q = 15.3%, Figure 3E), as may be expected, as our $^{15}N-^{1}H$ RDCs do not provide restraints for non-adenosine residues.

We have presented a new experiment that significantly extends the size limit for RNA RDC measurement. Studies with a 36-nucleotide RNA show that this method gives results consistent with existing methods that utilize an $S^{3}E$ element and affords data sufficient to define the interhelical angle for RNAs containing as few as three adenosines (six RDCs) per helix. In most cases, large RNAs should contain sufficient adenosine signals in each secondary structure element (e.g., RRE^{232A}, Supporting Information Figure S1D). For unfavorable sequences, additional A:U base pairs may be introduced by mutagenesis, perhaps in combination with lrAID sequences,[7] to ensure maximal signal dispersion and resolution. We expect the VF-HMQC approach to be applicable to RNAs on the order of hundreds of nucleotides, thereby providing access to higher quality structures of larger RNAs than previously possible.

MATERIALS AND METHODS

***In Vitro* Transcription.** RNA molecules were produced by *in vitro* transcription using T7 RNA polymerase[45] in 7.5 mL reactions, containing 50 μg of PCR-amplified DNA template (RRE^{232A}) or 2.5 nmol of annealed DNA template (SLC^{A}), 2 mM spermidine, 80 mM Tris·HCl (pH 8.5), 2 mM DTT, 20% (v/v) DMSO, 0.5 mg of T7 RNA polymerase, 10−20 mM $MgCl_2$, and 3−6 mM NTPs. DNA templates are 2′-*O*-methyl-modified at the last two nucleotides of the 5′ end to improve 3′ end homogeneity of transcribed RNA.[46,47] ^{15}N-Labeled samples were prepared with [U-98−99% ^{15}N]-ATP, [U-97%+ ^{2}H]-CTP, [U-97%+ ^{2}H]-GTP, and [U-97%+ ^{2}H]-UTP (CIL). ^{13}C-Labeled samples were prepared with [U ^{13}C]-ATP, [U ^{13}C]-CTP, [U ^{13}C]-GTP, and [U ^{13}C]-UTP (CIL). Reactions were incubated at 37 °C for 4 h before quenching by addition of EDTA. RNA was purified by electrophoresis on urea-containing polyacrylamide denaturing gels (SequaGel, National Diagnostics) using a FisherBiotech DNA sequencing system at 20 W overnight, before electroelution using the Elutrap system (Whatman) at 120 V overnight. The eluted RNAs were washed with 2 M NaCl and then desalted using a 30 kDa (RRE^{232A}) or 3 kDa (SLC^{A}) MWCO Amicon Ultra-4 Centrifugal Filter Device (Millipore). The concentration of each sample was determined by measuring the optical absorbance at 260 nm. Samples were exchanged into D_2O (99.96%; CIL) by two rounds of lyophilization before dissolution in NMR buffer.

NMR Sample Preparation. RRE^{232A} NMR samples (160 μL of ∼1.5 mM RNA in D_2O) were prepared in a 3 mm NMR tube with 20 mM Tris−d11 buffer (pH 7.4), 140 mM KCl, and 1 mM $MgCl_2$. SLC^{A} NMR samples (500 μL of ∼500 μM RNA in D_2O) were prepared in a 5 mm NMR tube with 20 mM Tris−d11 buffer (pH 7.4). For aligned samples, Pf1 phage (ASLA Biotech) was exchanged into D_2O by repeated washing using a 30 kDa MWCO Amicon Ultra-4 Centrifugal Filter Device (Millipore). Phage concentration was estimated by the quadrupolar splitting of the D_2O signal.[48] Lyophilized RNA was resuspended in 10−15 mg/mL of Pf1 in D_2O. To simplify analysis, ^{15}N and ^{13}C-labeled SLC^{A} were combined (500 μL total volume with ∼250 μM of each RNA) for the aligned sample.

NMR Experiments. All experiments were performed at 308 K on a Bruker AVANCE III HD spectrometer at 600.13 MHz. SOFAST-HMQC,[24,25] $S^{3}E$,[31] and ARTSY[22] experiments were performed as previously described. Spectra were processed using NMRFx[49] and NMRPipe.[50] Chemical shifts and NOEs were assigned using NMRViewJ[51] with a combination of $^{1}H-^{1}H$ NOESY, $^{1}H-^{1}H$ TOCSY, and $^{13}C-^{1}H$ HMQC spectra, utilizing predicted chemical shifts[52,53] and in-house scripts. Relaxation data was processed and analyzed using Bruker TopSpin v3.5.

Structure Calculation. Structures were calculated with CYANA[54] (v2.1 and 3.97) using NOE, H-bond, and database derived interphosphate distance restraints, as described previously.[10] Structures with low target functions were then subjected to rounds of conjugate gradient minimization using RDC restraints with increasing weight coefficients (to a maximum of 0.1). $^{15}N-^{1}H$ RDCs were weighted 14.45 times greater than $^{13}C-^{1}H$ restraints.

ASSOCIATED CONTENT

Supporting Information

The Supporting Information is available free of charge on the ACS Publications website at DOI: 10.1021/jacs.8b03298.

Supplementary Figures 1−8 and Appendix 1 (PDF)
SLC^{A} chemical shifts (TXT)
VF-HMQC pulse sequence (TXT)
SLC^{A} atomic coordinates calculated using $^{13}C-^{1}H$ RDCs (PDB)
SLC^{A} atomic coordinates calculated using $^{15}N-^{1}H$ RDCs (PDB)

AUTHOR INFORMATION

Corresponding Authors

*janm@umbc.edu
*summers@hhmi.umbc.edu

ORCID

Jan Marchant: 0000-0002-2418-6247
Ad Bax: 0000-0002-9809-5700
Michael F. Summers: 0000-0003-4267-4380

Notes

The authors declare no competing financial interest.

ACKNOWLEDGMENTS

The authors would like to acknowledge Daniel Morris, Stanley Wang, Colin O'Hern, and Sophia Abbott for preparation of the RNA used in this work, together with HHMI staff at UMBC for their general assistance. Funding from the NIH (U54 GM103297 to J.M.; GM42561 to M.F.S.; Intramural Research Program of the NIDDK and the Intramural Antiviral Target Program of the Office of the Director, NIH, to A.B.) and HHMI is gratefully acknowledged.

REFERENCES

(1) Caprara, M. G.; Nilsen, T. W. *Nat. Struct. Biol.* **2000**, *7* (10), 831−3.
(2) Alvarado, L. J.; LeBlanc, R. M.; Longhini, A. P.; Keane, S. C.; Jain, N.; Yildiz, Z. F.; Tolbert, B. S.; D'Souza, V. M.; Summers, M. F.; Kreutz, C.; Dayie, T. K. *ChemBioChem* **2014**, *15* (11), 1573−7.
(3) Allain, F. H.-T.; Varani, G. *J. Mol. Biol.* **1997**, *267*, 338−351.
(4) Lukavsky, P. J.; Puglisi, J. D. *Methods Enzymol.* **2005**, *394*, 399−415.
(5) D'Souza, V.; Dey, A.; Habib, D.; Summers, M. F. *J. Mol. Biol.* **2004**, *337* (2), 427−42.
(6) Miyazaki, Y.; Irobalieva, R. N.; Tolbert, B. S.; Smalls-Manty, A.; Iyalla, K.; Loeliger, K.; D'Souza, V.; Khant, H.; Schmid, M. F.; Garcia, E.; Telesnitsky, A.; Chiu, W.; Summers, M. F. *J. Mol. Biol.* **2010**, *404*, 751−772.
(7) Lu, K.; Heng, X.; Garyu, L.; Monti, S.; Garcia, E.; Kharytonchyk, S.; Dorjsuren, B.; Kulandaivel, G.; Jones, S.; Hiremath, A.; Sachin

DOI: 10.1021/jacs.8b03298
J. Am. Chem. Soc. 2018, 140, 6978−6983

Divakaruni, S.; LaCotti, C.; Barton, S.; Tummillo, D.; Hosic, A.; Edme, K.; Albrecht, S.; Telesnitsky, A.; Summers, M. F. *Science* **2011**, *334*, 242−245.
(8) Keane, S. C.; Heng, X.; Lu, K.; Kharytonchyk, S.; Ramakrishnan, V.; Carter, G.; Barton, S.; Hosic, A.; Florwick, A.; Santos, J.; Bolden, N. C.; McCowin, S.; Case, D. A.; Johnson, B. A.; Salemi, M.; Telesnitsky, A.; Summers, M. F. *Science* **2015**, *348* (6237), 917−21.
(9) Davis, J. H.; Tonelli, M.; Scott, L. G.; Jaeger, L.; Williamson, J. R.; Butcher, S. E. *J. Mol. Biol.* **2005**, *351*, 371−382.
(10) Tolbert, B. S.; Miyazaki, Y.; Barton, S.; Kinde, B.; Starck, P.; Singh, R.; Bax, A.; Case, D. A.; Summers, M. F. *J. Biomol. NMR* **2010**, *47*, 205−219.
(11) Mollova, E. T.; Hansen, M. R.; Pardi, A. *J. Am. Chem. Soc.* **2000**, *122*, 11561−11562.
(12) Ying, J.; Grishaev, A.; Latham, M. P.; Pardi, A.; Bax, A. *J. Biomol. NMR* **2007**, *39*, 91−96.
(13) Lukavsky, P. J.; Kim, I.; Otto, G. A.; Puglisi, J. D. *Nat. Struct. Mol. Biol.* **2003**, *10*, 1033−1038.
(14) Staple, D. W.; Butcher, S. E. *J. Mol. Biol.* **2005**, *349*, 1011−1023.
(15) Kim, N. K.; Zhang, Q.; Zhou, J.; Theimer, C. A.; Peterson, R. D.; Feigon, J. *J. Mol. Biol.* **2008**, *384* (5), 1249−61.
(16) Skrisovska, L.; Bourgeois, C. F.; Stefl, R.; Grellscheid, S. N.; Kister, L.; Wenter, P.; Elliott, D. J.; Stevenin, J.; Allain, F. H. *EMBO Rep.* **2007**, *8* (4), 372−9.
(17) Zhang, Q.; Sun, X.; Watt, E. D.; Al-Hashimi, H. M. *Science* **2006**, *311*, 653−656.
(18) Zhang, Q.; Stelzer, A. C.; Fisher, C. K.; Al-Hashimi, H. M. *Nature* **2007**, *450*, 1263−1267.
(19) Tjandra, N.; Bax, A. *Science* **1997**, *278* (5340), 1111−1114.
(20) Prestegard, J. H.; al-Hashimi, H. M.; Tolman, J. R. *Q. Rev. Biophys.* **2000**, *33* (4), 371−424.
(21) Bax, A.; Kontaxis, G.; Tjandra, N. *Methods Enzymol.* **2001**, *339*, 127−74.
(22) Ying, J.; Wang, J.; Grishaev, A.; Yu, P.; Wang, Y. X.; Bax, A. *J. Biomol. NMR* **2011**, *51* (1−2), 89−103.
(23) Wijmenga, s. s.; van Buurehn, B. N. M. *Prog. Nucl. Magn. Reson. Spectrosc.* **1998**, *32*, 287−387.
(24) Schanda, P.; Brutscher, B. *J. Am. Chem. Soc.* **2005**, *127* (22), 8014−5.
(25) Sathyamoorthy, B.; Lee, J.; Kimsey, I.; Ganser, L. R.; Al-Hashimi, H. *J. Biomol. NMR* **2014**, *60* (2−3), 77−83.
(26) Prestegard, J. H. *Nat. Struct. Biol.* **1998**, *5*, 517−522.
(27) Geen, H.; Freeman, R. *J. Magn. Reson.* **1991**, *93*, 93−141.
(28) Garwood, M.; Ke, Y. *J. Magn. Reson.* **1991**, *94*, 511−525.
(29) Marion, D.; Ikura, M.; Tschudin, R.; Bax, A. *J. Magn. Reson.* **1989**, *85*, 393−399.
(30) Shaka, A. J.; Barker, P. B.; Freeman, R. *J. Magn. Reson.* **1985**, *64*, 547−552.
(31) Zidek, L.; Wu, H.; Feigon, J.; Sklenar, V. *J. Biomol. NMR* **2001**, *21* (2), 153−60.
(32) Fonseca Guerra, C.; Matthias Bickelhaupt, F.; Snijders, J. G.; Baerends, E. J. *J. Am. Chem. Soc.* **2000**, *122*, 4117−4128.
(33) Ward, J. M.; Skrynnikov, N. R. *J. Biomol. NMR* **2012**, *54* (1), 53−67.
(34) Sherpa, C.; Rausch, J. W.; Le Grice, S. F.; Hammarskjold, M. L.; Rekosh, D. *Nucleic Acids Res.* **2015**, *43* (9), 4676−86.
(35) Meissner, A.; Duus, J. O.; Sorensen, O. W. *J. Biomol. NMR* **1997**, *10* (1), 89−94.
(36) Stueber, D.; Grant, D. M. *J. Am. Chem. Soc.* **2002**, *124* (35), 10539−51.
(37) Bax, A.; Max, D.; Zax, D. *J. Am. Chem. Soc.* **1992**, *114* (17), 6923−6925.
(38) Griesinger, C.; Sørensen, O. W.; Ernst, R. R. *J. Chem. Phys.* **1986**, *85* (12), 6837−6852.
(39) Otting, G.; Messerle, B. A.; Soler, L. P. *J. Am. Chem. Soc.* **1996**, *118*, 5096−5102.
(40) Otting, G.; Messerle, B. A.; Soler, L. P. *J. Am. Chem. Soc.* **1997**, *119*, 5425−5434.
(41) Garwood, M.; DelaBarre, L. *J. Magn. Reson.* **2001**, *153* (2), 155−77.
(42) Zweckstetter, M.; Bax, A. *J. Biomol. NMR* **2002**, *23* (2), 127−37.
(43) Bailor, M. H.; Musselman, C.; Hansen, A. L.; Gulati, K.; Patel, D. J.; Al-Hashimi, H. M. *Nat. Protoc.* **2007**, *2* (6), 1536−46.
(44) Fitzkee, N. C.; Bax, A. *J. Biomol. NMR* **2010**, *48* (2), 65−70.
(45) Milligan, J. F.; Groebe, D. R.; Witherell, G. W.; Uhlenbeck, O. C. *Nucleic Acids Res.* **1987**, *15* (21), 8783−9798.
(46) Kao, C.; Zheng, M.; Rüdisser, S. *RNA* **1999**, *5*, 1268−1272.
(47) Helmling, C.; Keyhani, S.; Sochor, F.; Furtig, B.; Hengesbach, M.; Schwalbe, H. *J. Biomol. NMR* **2015**, *63* (1), 67−76.
(48) Hansen, M. R.; Mueller, L.; Pardi, A. *Nat. Struct. Biol.* **1998**, *5*, 1065−1074.
(49) Norris, M.; Fetler, B.; Marchant, J.; Johnson, B. A. *J. Biomol. NMR* **2016**, *65*, 205−216.
(50) Delaglio, F.; Grzesiek, S.; Vuister, G. W.; Zhu, G.; Pfeifer, J.; Bax, A. *J. Biomol. NMR* **1995**, *6*, 277−293.
(51) Johnson, B. A.; Blevins, R. A. *J. Biomol. NMR* **1994**, *4*, 603−614.
(52) Barton, S.; Heng, X.; Johnson, B. A.; Summers, M. F. *J. Biomol. NMR* **2013**, *55* (1), 33−46.
(53) Brown, J. D.; Summers, M. F.; Johnson, B. A. *J. Biomol. NMR* **2015**, *63* (1), 39−52.
(54) Güntert, P.; Mumenthaler, C.; Wüthrich, K. *J. Mol. Biol.* **1997**, *273*, 283−298.

DOI: 10.1021/jacs.8b03298
J. Am. Chem. Soc. 2018, 140, 6978−6983